Impact of the Topological Surface State on the Thermoelectric Transport in Sb_2Te_3 Thin Films

Nicki F. Hinsche,[*,†] Sebastian Zastrow,[‡] Johannes Gooth,[‡] Laurens Pudewill,[‡] Robert Zierold,[‡] Florian Rittweger,[§] Tomáš Rauch,[†] Jürgen Henk,[†] Kornelius Nielsch,[‡] and Ingrid Mertig[†,§]

[†]Institute of Physics, Martin Luther University Halle-Wittenberg, D-06099 Halle, Germany, [‡]Institute of Nanostructure and Solid State Physics, Universität Hamburg, Jungiusstrasse 11, D-20355 Hamburg, Germany, and [§]Max Planck Institute of Microstructure Physics, Weinberg 2, D-06120 Halle, Germany

ABSTRACT *Ab initio* electronic structure calculations based on density functional theory and tight-binding methods for the thermoelectric properties of *p*-type Sb_2Te_3 films are presented. The thickness-dependent electrical conductivity and the thermopower are computed in the diffusive limit of transport based on the Boltzmann equation. Contributions of the bulk and the surface to the transport coefficients are separated, which enables to identify a clear impact of the topological surface state on the thermoelectric properties. When the charge carrier concentration is tuned, a crossover between a surface-state-dominant and a Fuchs-Sondheimer transport regime is achieved. The calculations are corroborated by thermoelectric transport measurements on Sb_2Te_3 films grown by atomic layer deposition.

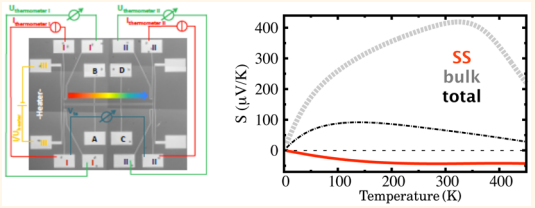

KEYWORDS: topological insulators · thermoelectrics · thin films · density functional theory (DFT) · atomic layer deposition (ALD) · surface states · thermopower · four-terminal measurements

Almost all proposed three-dimensional (3D) Z_2 topological insulators (TIs)[1,2] are efficient thermoelectric materials. That is not by coincidence, since the link between an efficient thermoelectric material and the topological character is the inverted band gap.[3,4] The last is due to spin–orbit coupling which switches parity of the bands and leads, if strong enough, to narrow band gaps which are favorable for efficient room-temperature thermoelectrics. Usually, strong spin–orbit coupling is mediated by heavy elements, which in turn also tend to reduce the material's lattice thermal conductivity, another requirement for desirable thermoelectrics.

In the early 90s, Hicks and Dresselhaus[5,6] proposed the concept of low-dimensionality to increase further the thermoelectric efficiency; primarily in thin films, the thermopower *S* should be enlarged. However, in contrast to previous theoretical model calculations,[7,8] decreased values of *S* were found experimentally[9−11] for Bi_2Te_3 and Sb_2Te_3 thin films and were recently corroborated by both model[12,13] and *ab initio* calculations[4] of our groups.

Thus, to resolve this discrepancy, the potential impact of the surface state (SS) of TIs on thermoelectricity needs to be investigated in more detail. In this Article, we present *ab initio* calculations and transport measurements of the thermoelectric properties of Sb_2Te_3 films at varying thickness, temperature, and charge carrier concentration.

RESULTS

Theoretical Results. In the following, we discuss the doping- and temperature-dependent electrical conductivity and thermopower, as shown in Figure 1, exemplary for a Sb_2Te_3 film with thickness of 18 quintuple-layer (QL), *i.e.*, about 18 nm. A discussion of films with other thicknesses is given in the Supporting Information.[14]

The converged electronic structure results serve as input to obtain the thermoelectric transport properties at temperature *T* and fixed extrinsic charge carrier concentration *p* by solving the linearized Boltzmann equation in relaxation time approximation (RTA).[15] By using special projection techniques,[4] we distinguish between contributions from bulk states (gray

* Address correspondence to nicki.hinsche@physik.uni-halle.de.

Received for review February 7, 2015 and accepted March 31, 2015.

Published online March 31, 2015
10.1021/acsnano.5b00896

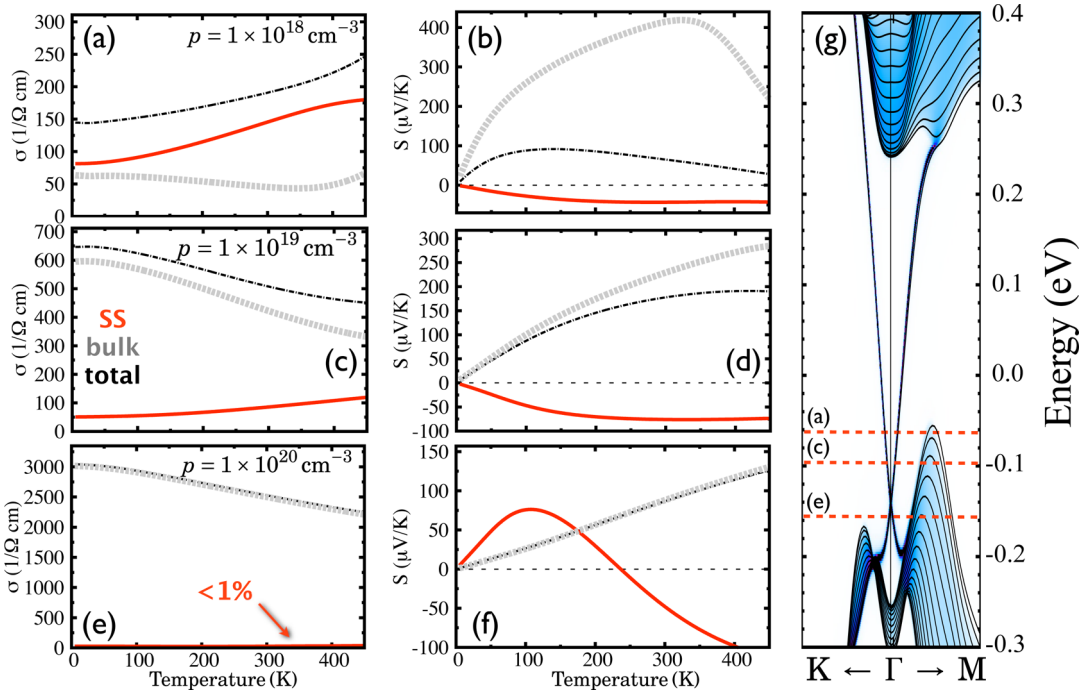

Figure 1. Electrical conductivity (a, c, and e) and thermopower (b, d, and f) in dependence on temperature for three distinct hole concentrations at a film thickness of 18 QL. Hole concentration $n = 1 \times 10^{18}$ cm^{-3} in (a) and (b), $p = 1 \times 10^{19}$ cm^{-3} in (c) and (d), $p = 1 \times 10^{20}$ cm^{-3} in (e) and (f). Pure bulk contributions are represented by gray dashed lines; the contribution of the surface states is given by red solid lines, while black dash-dotted lines show the total contribution of the sample. In (g) the band structure of the 18 QL Sb_2Te_3 film is shown around the fundamental band gap. Thin red dashed lines indicate the position of the chemical potential μ at zero temperature.

dashed lines), SSs (red solid lines), and the total contribution (black dash-dotted line), defined as $\sigma_{tot} = \sigma_{bulk} + \sigma_{SS}$ and $S_{tot} = (\sigma_{bulk}S_{bulk} + \sigma_{SS}S_{SS})/\sigma_{tot}$. Three typical charge carrier concentrations are chosen to reflect the overall behavior of the transport properties. Only *p*-type thin films will be discussed because Sb_2Te_3 is inherently *p*-type conductive[16,17] due to intrinsic defects, *i.e.*, Sb vacancies, Sb_{Te} antisites, and $Sb-Te_1$ exchange defects.

Due to the fact that a 3D TI offers robust metallic SSs (we denote the SS metallic, as it shows clear transport signatures of a conventional metal) within the insulating bulk band gap, an enhanced electrical conductivity of the entire system compared to a conventional insulator is expected for very small charge carrier concentrations, *i.e.*, if the chemical potential is situated in or nearby the bulk band gap. The latter scenario is shown in Figure 1a for a *p*-type doping of $p = 1 \times 10^{18}$ cm^{-3}. At low temperatures, the contribution σ_{SS} of the SS (red solid line) is already larger than the bulk contribution σ_{bulk}. With increasing temperature, the chemical potential shifts into the band gap, thereby decreasing σ_{bulk} until bipolar conduction contributes at about $T = 300$ K. In contrast, σ_{SS} increases monotonically with temperature. The latter can easily be understood, having in mind that for a two-dimensional system, *i.e.*, the SS, the transport distribution function (TDF) scales as $\Sigma(\mu) \propto dl_F \times v$, where dl_F is the circumference of the Fermi circle at chemical potential μ. For energies close to the Dirac point, v_{SS} is constant in energy, while $dl_F \propto E$. Consequently, the TDF is linear in energy. Small deviations from the latter arise at about $E \approx 0.1$ eV and are attributed to the hexagonal warping of the Fermi surface.

The impact of the SS on the total thermopower, as shown in Figure 1b, is even more remarkable. While the bulk contribution S_{bulk} shows the typical behavior for a *p*-type narrow-band gap semiconductor with a maximum of $S_{bulk} \approx 410$ μV/K at $T = 325$ K, the contribution of the SS shows the expected metallic behavior with small values of $S_{SS} \leq -50$ μV/K. The negative sign stems from the mere fact that the SS above (below) the Dirac point mimics the slope of the band dispersion of conduction (valence) bands.

Summarizing, the influence of the SS leads to a clearly diminished total thermopower (black dash-dotted line). As a rule of thumb, assuming $S_{bulk} \gg S_{SS}$ yields $S_{tot} \approx S_{bulk}/(\eta + 1)$ with $\eta = \sigma_{SS}/\sigma_{bulk}$. The larger the contribution of the SS to the total electrical conductivity, the smaller the total thermopower S_{tot}.

The value of the total thermopower (65 μV/K at 300 K; black dashed-dotted line in Figure 1b) is reduced to less than one-fifth of the bulk value, which corroborates the above-noted estimation. We note that, within the RTA, the signature of the SS on S_{tot} relies to a certain extent on the ratio τ_{SS}/τ_{bulk} of the relaxation times. If $\tau_{bulk} \gg \tau_{SS}$, the reduction of the total thermopower due to the conducting SS would be much weaker than

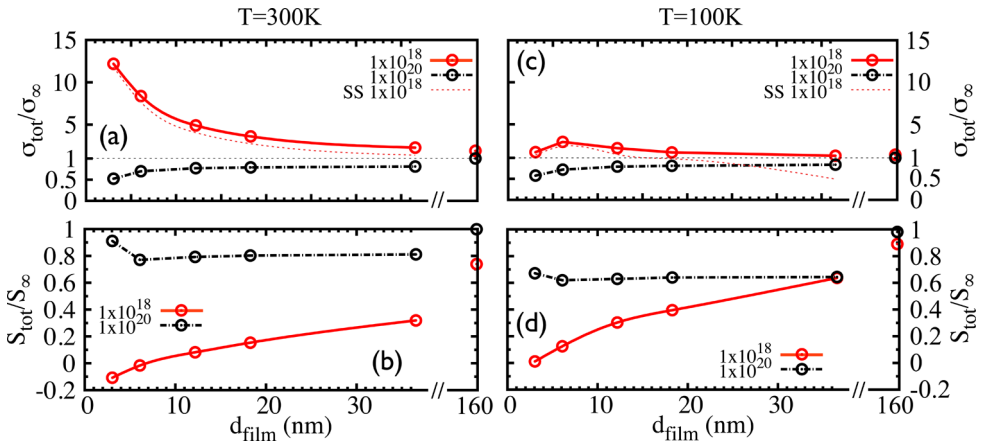

Figure 2. Thickness-dependent thermoelectric transport properties. Total electrical conductivity and thermopower at T = 300 K (a and b) and T = 100 K (c and d), respectively. The results are depicted for two distinct hole concentrations: $p = 1 \times 10^{18}$ cm^{-3} (red solid lines) and $p = 1 \times 10^{20}$ cm^{-3} (black dash-dotted lines). For the electrical conductivity in (a) and (c), the pure contribution of the surface state is given additionally as a thin dashed red line. All the transport properties are normalized to the bulk values σ_∞ and S_∞.

proposed. With regard to the backscattering protection of the SS, however, the opposite scenario $\tau_{SS} \gg \tau_{bulk}$ should be expected.[18]

For thermoelectric applications charge carrier concentration of $p = 1 \times 10^{19}$ cm^{-3} (*cf.* Figure 1, panels c and d) are more applicable. Here the contribution of the SS to σ_{tot} is smaller, compared to the low doped case, as the chemical potential is located closer to the Dirac point (*cf.* Figure 1c). Still, a reduction of the film's total thermopower by 45% to $S_{tot} \approx 187$ μV/K at T = 400 K compared to the bare bulk value is calculated due to the impact of the metallic SS (*cf.* Figure 1d).

In heavy p-doped samples, at $p = 1 \times 10^{20}$ cm^{-3}, as depicted in Figure 1, panels e and f, the absolute value of S_{SS} still reaches about 25 $(\Omega\text{cm})^{-1}$ at room temperature but is negligibly small compared to the bulk contribution. This is reflected in the thermopower, for which $S_{tot} \approx S_{bulk}$. Focusing on the SS contribution, the picture is more delicate. At low temperatures, S_{SS} is positive but decreases at elevated temperatures and changes sign at about T = 250 K. The latter is attributed to a shift of the chemical potential above the Dirac point, where the slope of both the TDF and S_{SS} change sign.

After discussing the temperature and doping-dependent thermoelectric transport properties for a film of 18 QL thickness, we now focus on the film thickness dependence of the transport properties at T = 300 K and T = 100 K, as shown in Figure 2. At room-temperature, two distinct transport regimes can be discussed with respect to the dependence of the charge carrier concentration of the films. At heavy p-doping ($p = 1 \times 10^{20}$ cm^{-3}, black dash-dotted lines in Figure 2), the film behaves almost metallic without significant influence of the topological SS on the transport properties. With increasing film thickness the normalized electrical conductivity at room temperature (*cf.* Figure 2a) tends asymptotically to the bulk value as $(\sigma_{tot}/\sigma_\infty) \sim (1 + (3\nu\tau/8d))^{-1}$ in accordance with the Fuchs-Sondheimer theory.[19,20] While derived to describe surfaces the Fuchs-Sondheimer theory does not account for the influence of SSs and quantum size effects. As previously described, these can be probed at low charge carrier concentrations ($p = 1 \times 10^{18}$ cm^{-3}, red solid lines in Figure 2). As shown in Figure 2a, the behavior of the total electrical conductivity than differs evidently from the Fuchs-Sondheimer limit. At low film thickness we find enhanced values of $(\sigma_{tot}/\sigma_\infty) \approx 12$. Obviously the contributions of the SSs dominate the transport and lift the total electrical conductivity above the bulk limit. As indicated in Figure 2a, the contribution of the SS to the total transport exceeds 90% (*cf.* the thin red dashed lines). A comparable crossover between surface state-dominated and Fuchs-Sondheimer transport was reported for ultrathin copper films.[21] Generally speaking, for film thicknesses above 18 QL thickness, the ***k***-dependency and spatial distribution of the surface states is fully established. Thus, the surface contribution to the transport properties remain robust for thicker films and the TDF scales as $\Sigma_{SS}(d) \sim (1/d)$. Quantum confinement effects are hardly visible for the 160 QL film, *i.e.*, $\sigma_{bulk}(d) \approx \sigma_\infty$ and $\sigma_{tot}(d) \approx \sigma_\infty + (\sigma_{SS}/d)$.

The dependence of the normalized total thermopower on the film thickness is presented in Figure 2b,d. Keeping in mind the aforementioned relation $S_{tot}/S_\infty \approx (\sigma_\infty + \sigma_{SS} \times (S_{SS}/S_\infty))/\sigma_{tot}$, $S_{tot}/S_\infty \leq 1$ can be expected for a broad range of temperatures and doping in the thin TI films. (We note that there is a difference of S_{bulk} and S_∞, which are the bulk contribution to a thin film and the contribution of a perfect infinite bulk, respectively. However, $S_{bulk} = S_\infty$ is used in this estimation and is valid for qualitative discussions.) This is related to the mere fact, that in a TI the SS is metallic, hence showing small values of $|S_{SS}|$, while the bulk is insulating yielding large values of $|S_\infty|$. The position of the Dirac point near

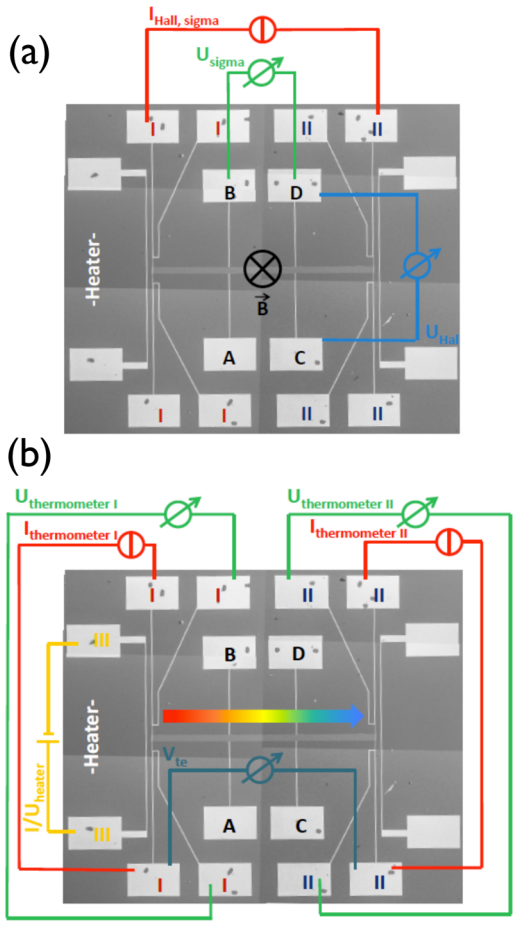

Figure 3. Device for electrical conductivity σ and Hall measurements (a) as well as for determining the Seebeck coefficient $S = V_{th}/(T_I - T_{II})$ (b) of a Sb_2Te_3 thin film. The magnetic field B is applied perpendicular to the film plane. Bright lines are lithographically defined metal lines used as heater, as ohmic inner electrodes for electric measurements and as resistive thermometers, as indicated (see Methods for details).

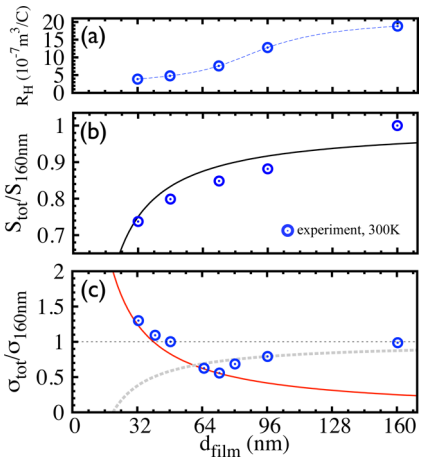

Figure 4. Measured thickness dependent thermoelectric transport properties at room temperature. Shown (as blue dots) is the normalized total thermopower (b) and the normalized total electrical conductivity (c) for varying film thickness. The charge carrier concentration varies monotonically with film thickness (a). Hence, the two transport regimes are superimposed in the experiment. The surface-state dominant regime (red solid line) and a Fuchs-Sondheimer transport regime (gray dashed line). The total thermopower (b) is always reduced due to the contribution of the surface-states.

the band edge, *i.e.*, the case in Sb_2Te_3 and Bi_2Te_3, leads moreover to opposite signs of S_{SS} and S_∞, further reducing S_{tot}/S_∞.

Occasionally, the bulk and the SS's contribution have the same sign and $S_{SS} > S_\infty$, leading to an enlarged $S_{tot}/S_\infty > 1$. The latter scenario is seen in Figure 1f for a heavily *p*-doped sample at temperatures lower than $T = 180$ K. However, as these situations occur only if the bulk is metallic, *i.e.*, $\sigma_{bulk} \gg \sigma_{SS}$, the total thermopower will not exceed the bulk limit considerably, yielding $S_{tot} \approx S_\infty$.

Experimental Results. To support our theoretical findings at room temperature, experimental four-terminal measurements (see Figure 3 and Methods) on the normalized total electrical conductivity and total thermopower at varying Sb_2Te_3 film thickness are presented in Figure 4. As can be seen from Figure 4b, the total thermopower tends asymptotically toward the bulk limit for increasing film thickness, *i.e.*, decreasing influence of the SSs, in accordance to the theoretical calculations in Figure 2b (preferably red solid line). Obviously the measured Hall coefficient R_H is not a constant with the film thickness (Figure 4a). Within a two channel model for R_H[14,22] and mobilities $\mu_{SS} \approx \mu_{bulk}$,[14,23] the charge carrier concentration *p* of the thin films slightly varies monotonically with the number of deposited layers, too. That allows for direct observation of the transition between the surface-state-dominant and Fuchs-Sondheimer transport regime of the total electrical conductivity, shown in Figure 4c.

At low film thickness, $d < 48$ nm and still low enough charge carrier concentrations the SSs noticeably influence the transport, *i.e.*, the normalized total electrical conductivity is higher than expected from the bare bulk sample (indicated by red solid lines). With increasing film thickness, the influence of the SSs is suppressed and bulk states dominate the transport. Nevertheless, the low charge carrier concentrations allow to see influences in the thermopower even at large film thicknesses, as pointed out in Figure 2b. Starting from a quantum mechanical approach, a Fuchs-Sondheimer transport regime can be expected (indicated by gray dashed lines), with the normalized total electrical conductivity tending to the bulk value for large film thickness. Clearly the measured data supports qualitatively all aspects of the theoretical calculations; hence, $\mu_{SS} \approx \mu_{bulk}$ is strongly expected.

To close our discussions, we point to the low temperature case of $T = 100$ K shown in Figure 2b,d. While the main trends remain and the same conclusions as for the room-temperature case can be drawn, the influence of the SS on the total electrical

conductivity being diminished (*cf.* Figure 2c). Two facts lead to this result: (*i*) the chemical potential is located deeper in the valence bands for a given charge carrier concentration and (*ii*) the broadening of the Fermi–Dirac distribution in eq 1 is reduced. Both facts lead to a reduced influence of the SSs located in the fundamental band gap. Deviations are only found for ultrathin films of 3 QL thickness, for which the hybridization of the SSs at opposite sides of the film opens up gaps in the SS bands; at low temperature both the SS and the bulk interior behave then like a conventional semiconductor.[8,12,14]

CONCLUSION

Combining quantum theoretical methods and experimental techniques on thin-film Sb_2Te_3, we reproduced and clarified the reduction the total thermopower found in various experiments on thin-film thermoelectric TIs.[9−11] By means of *ab initio* electronic structure calculations based on density functional theory, we discussed the thermoelectric properties of the *p*-type TI Sb_2Te_3 for various film thicknesses and temperatures. The topologically protected surface-state leads to metallic conduction of the thin films even in the semiconducting regime. As shown by a separation of bulk and surface contributions, the latter leads to a strong reduction of the total measured thermopower of the thin films. This reduction is present in a wide range of film thicknesses and doping. When we vary the charge carrier concentration a crossover between a surface-state-dominant and a Fuchs-Sondheimer transport regime is achieved. These two transport regimes, as well as a reduction of the total thermopower with decreasing film thickness are confirmed by thermoelectric transport measurements on atomic layer deposited Sb_2Te_3 thin films. To gain a thermoelectric benefit from thin film topological insulators, gapping the surface state at low temperatures and charge carrier concentrations seems to be the only favorable ansatz.

METHODS

Computational Details. The transport properties of the Sb_2Te_3 films are calculated in the diffusive limit of transport by means of the semiclassical Boltzmann equation in relaxation time approximation (RTA).[15,24] Within this approximation we assume that the attached heaters and metallic leads basically preserve the surface band structure.

The basis of the transport calculations, *i.e.*, the atomistic structure, was simulated by slabs of 15 to 800 atomic layers, *i.e.*, three −160 QL Sb_2Te_3. The experimental in-plane lattice parameter a^{hex}_{SbTe} = 4.264 Å and relaxed atomic positions[25] were used.

The electronic structures of the Sb_2Te_3 films were obtained by first-principles calculations within density functional theory (DFT), as implemented in the QuantumEspresso code.[26] Fully relativistic, norm-conserving pseudopotentials were used; exchange and correlation effects were accurately accounted for by the local density approximation (LDA).[27]

Subsequently, the first-principles electronic structures were mapped onto tight-binding Hamiltonians.[28,29] The resulting band structures were checked against our first-principles Korringa-Kohn-Rostoker[24,30] and QuantumEspresso results and yield fine agreement, in particular for the energy range near the fundamental band gap.

The electronic structures serves as an input to obtain the thermoelectric transport properties, using the layer-resolved transport distribution function (TDF) $\Sigma_i(\mu) = \mathscr{L}_i^{(0)}(\mu, 0)$.[31] The generalized conductance moments $\mathscr{L}_i^{(n)}(\mu, T)$ are defined as

$$\mathscr{L}_i^{(n)}(\mu,T) = \frac{\tau}{(2\pi)^2}\sum_\nu \int \mathrm{d}^2\mathbf{k}\ |v^\nu_{\mathbf{k}}|^2 \mathscr{P}^i_{\mathbf{k}}\ (E^\nu_{\mathbf{k}} - \mu)^n \left(-\frac{\partial f(\mu,T)}{\partial E}\right)_{E=E^\nu_{\mathbf{k}}} \quad (1)$$

$v^\nu_{\mathbf{k}}$ denotes the group velocities in the directions of the hexagonal basal plane and $\mathscr{P}^i_{\mathbf{k}}$ is the layer-resolved probability amplitude of a Bloch state, which allows for spatial decomposition of the transport properties.[32] Details on this projection technique are published elsewhere.[4] The relaxation time for Sb_2Te_3 was fitted to experimental data and chosen constant with absolute value τ = 12 fs with respect to wave vector $\boldsymbol{k}$ and energy on the scale of k_BT.[24] The influence of electron–phonon coupling was theoretically and experimentally found to be very weak and is discussed in detail in ref 4. Assuming stoichiometric samples, exchange-defects of Sb and Te_1 are the most probable scattering centers to be expected.[16] Thus, electron-impurity scattering will dominate. We checked the state-dependency of electron-impurity relaxation time $\tau_{\boldsymbol{k}}$ in Born approximation[14] and found a constant Brillouin zone averaged value of τ to be a reasonable approximation. The temperature- and doping-dependent in-plane electrical conductivity σ and thermopower *S* read

$$\sigma = 2e^2\mathscr{L}^{(0)}(\mu,T) \quad \text{and} \quad S = \frac{1}{eT}\frac{\mathscr{L}^{(1)}(\mu,T)}{\mathscr{L}^{(0)}(\mu,T)} \quad (2)$$

for given chemical potential μ at temperature *T* and fixed extrinsic carrier concentration.

The combination of first-principles and related tight-binding calculations allows for dense adaptive k-point meshes to ensure the convergence of eq 1.[30,33] The calculation consists of more than 500 points in a piece of the 2D Fermi surface in the irreducible part of the Brillouin zone (BZ).

Experimental Details. The Sb_2Te_3 thin films were grown on silicon wafers with a top layer of 300 nm SiO_2 *via* Atomic Layer Deposition (ALD) at substrate temperatures of 353 K. $(Et_3Si_2)Te$ and $SbCl_3$ were used as precursors at source temperatures of 350 and 328 K, respectively.[34] For the transport measurements, the Sb_2Te_3 thin films were deposited on a lithographically prepatterned Hall bar, which was defined *via* laser beam lithography and subsequent developing of the exposed photoresist. Contacts to the hall bars were defined in a second lithography step, prior to sputter deposition of Ti/Pt metal contacts. The thickness t and lateral dimensions (length l, width w) of the films were obtained by Atomic Force Microscopy and SEM images, respectively (*cf.* Supporting Information). The Hall resistance $R_H = U_{C,D}/I_{I,II}$ of the films was determined with standard lock-in technique. A constant ac current with an amplitude of $I_{I,II}$= 10 μA and frequency of 6 Hz was applied along the film stripe between contacts I and II and the voltage drop $U_{C,D}$ across the film width has been measured between contacts C and D, while sweeping a magnetic field from −3 to 3 T in 0.1 T steps (*cf.* Figure 3a). The magnetic field has been applied perpendicular to the film plane. The electrical conductivity has been calculated using $\sigma = [l/wt]/R_H$ where $R_H = U_{C,D}/I_{I,II}$ is the resistance of the film, measured in a four-point configuration between contacts B and D. To determine the Seebeck coefficient $S = V_{th}/\Delta T$ of the films the on-chip line heater generated a temperature difference ΔT across its length.

ΔT was measured by resistance thermometry using two metal four-probe thermometer lines (*I* and *II*) located at the film ends (*cf.* Figure 3b), which were driven by standard lock-in technique in a four-terminal configuration.[11,35] The metal lines for thermometry also served as electrodes for measuring V_{th}. Expected error bars for film thickness, thermopower and electrical conductivity are ~10%, ~16%, and ~7%, respectively.

Conflict of Interest: The authors declare no competing financial interest.

Acknowledgment. The authors acknowledge financial support by the Priority Programs SPP 1386 and SPP 1666 of DFG.

Supporting Information Available: Additional results on the doping- and temperature-dependent electrical conductivity and thermopower for other film thicknesses, informations on the electronic structure at varying film thickness, as well as structural analysis of the ALD grown thin films are available online. T This material is available free of charge *via* the Internet at http://pubs.acs.org.

REFERENCES AND NOTES

1. Zhang, H.; Liu, C.; Qi, X.; Dai, X.; Fang, Z.; Zhang, S. Topological Insulators in Bi_2Se_3, Bi_2Te_3 and Sb_2Te_3 with a Single Dirac Cone on the Surface. *Nat. Phys.* **2009**, *5*, 438–442.
2. Ando, Y. Topological Insulator Materials. *J. Phys. Soc. Jpn.* **2013**, *82*, 102001.
3. Kong, D.; Cui, Y. Opportunities in Chemistry and Materials Science for Topological Insulators and Their Nanostructures. *Nat. Chem.* **2011**, *3*, 845–849.
4. Rittweger, F.; Hinsche, N. F.; Zahn, P.; Mertig, I. Signature of the Topological Surface State in the Thermoelectric Properties of Bi_2Te_3. *Phys. Rev. B* **2014**, *89*, 035439.
5. Hicks, L.; Dresselhaus, M. Effect of Quantum-Well Structures on the Thermoelectric Figure of Merit. *Phys. Rev. B* **1993**, *47*, 12727–12731.
6. Hicks, L.; Harman, T.; Dresselhaus, M. Use of Quantum-Well Superlattices to Obtain a High Figure of Merit from Nonconventional Thermoelectric Materials. *Appl. Phys. Lett.* **1993**, *63*, 3230–3232.
7. Ghaemi, P.; Mong, R.; Moore, J. In-Plane Transport and Enhanced Thermoelectric Performance in Thin Films of the Topological Insulators Bi_2Te_3 and Bi_2Se_3. *Phys. Rev. Lett.* **2010**, *105*, 166603.
8. Takahashi, R.; Murakami, S. Thermoelectric Transport in Topological Insulators. *Semicond. Sci. Technol.* **2012**, *27*, 124005.
9. Boulouz, A.; Chakraborty, S.; Giani, A.; Delannoy, F.; Boyer, A.; Schumann, J. Transport Properties of V-Vi Semiconducting Thermoelectric BiSbTe Alloy Thin Films and Their Application to Micromodule Peltier Devices. *J. Appl. Phys.* **2001**, *89*, 5009–5014.
10. Peranio, N.; Eibl, O.; Nurnus, J. Structural and Thermoelectric Properties of Epitaxially Grown Bi_2Te_3 Thin Films and Superlattices. *J. Appl. Phys.* **2006**, *100*, 114306.
11. Zastrow, S.; Gooth, J.; Boehnert, T.; Heiderich, S.; Toellner, W.; Heimann, S.; Schulz, S.; Nielsch, K. Thermoelectric Transport and Hall Measurements of Low Defect Sb_2Te_3 Thin Films Grown by Atomic Layer Deposition. *Semicond. Sci. Technol.* **2013**, *28*, 035010.
12. Osterhage, H.; Gooth, J.; Hamdou, B.; Gwozdz, P.; Zierold, R.; Nielsch, K. Thermoelectric Properties of Topological Insulator Bi_2Te_3, Sb_2Te_3, and Bi_2Se_3 Thin Film Quantum Wells. *Appl. Phys. Lett.* **2014**, *105*, 123117.
13. Gooth, J.; Gluschke, J. G.; Zierold, R.; Leijnse, M.; Linke, H.; Nielsch, K. Thermoelectric Performance of Classical Topological Insulator Nanowires. *Semicond. Sci. Technol.* **2015**, *30*, 015015.
14. More informations can be found in the Supporting Information.
15. Mertig, I. Transport Properties of Dilute Alloys. *Rep. Prog. Phys.* **1999**, *62*, 237–276.
16. Thonhauser, T.; Jeon, G.; Mahan, G.; Sofo, J. Stress-Induced Defects in Sb_2Te_3. *Phys. Rev. B* **2003**, *68*, 205207.
17. Jiang, Y.; Sun, Y.; Chen, M.; Wang, Y.; Li, Z.; Song, C.; He, K.; Wang, L.; Chen, X.; Xue, Q.-K. Fermi-Level Tuning of Epitaxial Sb_2Te_3 Thin Films on Graphene by Regulating Intrinsic Defects and Substrate Transfer Doping. *Phys. Rev. Lett.* **2012**, *108*, 066809.
18. Roushan, P.; Seo, J.; Parker, C. V.; Hor, Y. S.; Hsieh, D.; Qian, D.; Richardella, A.; Hasan, M. Z.; Cava, R. J.; Yazdani, A. Topological Surface States Protected from Backscattering by Chiral Spin Texture. *Nature* **2009**, *460*, 1106.
19. Fuchs, K. Conductivity of Thin Metallic Films According to the Electron Theory of Metals. *Math. Proc. Cambridge Philos. Soc.* **1938**, *34*, 100.
20. Sondheimer, E. The Mean Free Path of Electrons in Metals. *Adv. Phys.* **1952**, *1*, 1–42.
21. Fedorov, D.; Zahn, P.; Mertig, I. Manifestation of Quantum Confinement in Transport Properties of Ultrathin Metallic Films. *Thin Solid Films* **2007**, *515*, 6921–6926.
22. Gonzalez, P.; Agapito, J. A.; Pardo, D. Two-Band Model Parameters Deduced from Hall Coefficient Measurements in Polycrystalline Films of SnTe. *J. Phys. C: Solid State Phys.* **1986**, *19*, 899.
23. Takagaki, Y.; Giussani, A.; Perumal, K.; Calarco, R.; Friedland, K.-J. Robust Topological Surface States in Sb_2Te_3 Layers as Seen from the Weak Antilocalization Effect. *Phys. Rev. B* **2012**, *86*, 125137.
24. Hinsche, N. F.; Yavorsky, B.; Mertig, I.; Zahn, P. Influence of Strain on Anisotropic Thermoelectric Transport in Bi_2Te_3 and Sb_2Te_3. *Phys. Rev. B* **2011**, *84*, 165214.
25. *Landolt-Börnstein New Series, Group III/41C*; Springer Verlag: Berlin, 1998.
26. Giannozzi, P.; Baroni, S.; Bonini, N.; Calandra, M.; Car, R.; Cavazzoni, C.; Ceresoli, D.; Chiarotti, G.; Cococcioni, M.; Dabo, I.; et al. QUANTUM ESPRESSO: A Modular and Open-Source Software Project for Quantum Simulations of Materials. *J. Phys.: Condens. Matter* **2009**, *21*, 395502.
27. Perdew, J. P. Self-Interaction Correction to Density-Functional Approximations for Many-Electron Systems. *Phys. Rev. B* **1981**, *23*, 5048–5079.
28. Rauch, T.; Flieger, M.; Henk, J.; Mertig, I. Nontrivial Interface States Confined Between Two Topological Insulators. *Phys. Rev. B* **2013**, *88*, 245120.
29. Rauch, T.; Flieger, M.; Henk, J.; Mertig, I.; Ernst, A. Dual Topological Character of Chalcogenides: Theory for Bi_2Te_3. *Phys. Rev. Lett.* **2014**, *112*, 016802.
30. Yavorsky, B. Y.; Hinsche, N. F.; Mertig, I.; Zahn, P. Electronic Structure and Transport Anisotropy of Bi_2Te_3 and Sb_2Te_3. *Phys. Rev. B* **2011**, *84*, 165208.
31. Mahan, G.; Sofo, J. The Best Thermoelectric. *Proc. Natl. Acad. Sci. U.S.A.* **1996**, *93*, 7436.
32. Zahn, P.; Binder, J.; Mertig, I.; Zeller, R.; Dederichs, P. Origin of Giant Magnetoresistance: Bulk or Interface Scattering. *Phys. Rev. Lett.* **1998**, *80*, 4309–4312.
33. Zahn, P.; Hinsche, N. F.; Yavorsky, B.; Mertig, I. Bi_2Te_3: Implications of the Rhombohedral k-Space Texture on the Evaluation of the In-Plane/Out-Of-Plane Conductivity Anisotropy. *J. Phys.: Condens. Matter* **2011**, *23*, 505504.
34. Pore, V.; Hatanpää, T.; Ritala, M.; Leskelä, M. Atomic Layer Deposition of Metal Tellurides and Selenides Using Alkylsilyl Compounds of Tellurium and Selenium. *J. Am. Chem. Soc.* **2009**, *131*, 3478–3480.
35. Bae, C.; Böhnert, T.; Gooth, J.; Lim, S.; Lee, S.; Kim, H.; Heimann, S.; Schulz, S.; Shin, H.; Nielsch, K. Thermopower Engineering of Bi_2Te_3 Without Alloying: The Interplay between Nanostructuring and Defect Activation. *Semicond. Sci. Technol.* **2014**, *29*, 064003.